Journal of
Materials Chemistry C

Accepted Manuscript

This article can be cited before page numbers have been issued, to do this please use: M. Hermann, R. Wu, D. C. Grenz, D. Kratzert, H. Li and B. Esser, *J. Mater. Chem. C*, 2018, DOI: 10.1039/C8TC00970H.

ROYAL SOCIETY OF CHEMISTRY

rsc.li/materials-c

View Article Online
DOI: 10.1039/C8TC00970H

Journal of Materials Chemistry C

ARTICLE

Thioether- and sulfone-functionalized dibenzopentalenes as n-channel semiconductors for organic field-effect transistors

Received 00th January 20xx,
Accepted 00th January 20xx

DOI: 10.1039/x0xx00000x

www.rsc.org/

Mathias Hermann,[a] Ruihan Wu,[b] David C. Grenz,[a] Daniel Kratzert,[c] Hanying Li*[b] and Birgit Esser*[a]

Dibenzo[*a*,*e*]pentalenes (DBPs) are promising candidates to be used as ambipolar or n-type semiconductors in organic field-effect transistors (OFETs). For n-channel conduction, low LUMO energy levels are required. Furthermore, a close molecular packing in the solid state is advantageous. Here we present thioether-functionalized DBPs with LUMO energies down to −3.47 eV as well as a DBP sulfone with a LUMO energy of −3.94 eV. X-ray crystallography revealed 1-D π-stacking or herringbone packing in the solid state with close intramolecular distances between the DBP cores. Two thio-DBPs and the DBP sulfone showed n-channel conduction in FET measurements on well-aligned crystals with electron mobilities of up to 0.18 $cm^2 V^{-1} s^{-1}$, up to date the highest reported values for n-channel conduction in DBP derivatives. The short synthetic route will in the future allow for facile access to a variety of thio- and sulfone-DBPs for n-channel or ambipolar semiconduction.

Introduction

Dibenzo[*a*,*e*]pentalene (DBP, **1**, Fig. 1) is a low bandgap, organic semiconductor. Its low bandgap is caused by the non-alternant nature of its π-system due to the presence of five-membered rings, which causes a shift in orbital energies.[1] Compared to acenes, solely consisting of six-membered rings, a lowered LUMO energy results, which has also been observed for many other non-alternant π-systems such as fullerenes,[2] pentalene derivatives,[3–6] indenofluorenes,[7,8] azulenes,[9,10] and others.[11] This makes DBPs of particular interest for an application as n-type or ambipolar semiconductors in organic field-effect transistors (OFETs). Compared to p-type materials, fewer n-type or ambipolar OFET-materials exist.[12–16] Several diacenopentalenes or other DBP derivatives have been investigated in p-channel OFETs.[17–20] To achieve a sufficiently low LUMO level for n-channel conduction between −3 eV and −4 eV, structural modification of the DBP core is necessary. Here, diacenopentalene dicarboximides[21] as well as the structurally related dicyanomethylene-substituted thienoquinoidals[22] have been investigated in n-channel OFETs. Instead of ring fusion, a lowering of the LUMO level can also be achieved through substitution.[23–25]

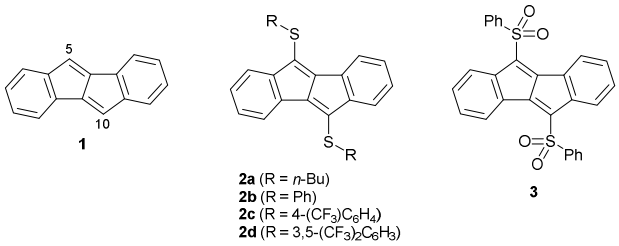

Fig. 1 Dibenzo[*a*,*e*]pentalene (DBP, **1**) and thio-DBPs **2a–d** as well as sulfone **3** investigated in this study.

We have recently shown that substituents at the 5,10-positions in DBP (Fig. 1) are particularly effective in lowering the LUMO energy.[23,25] Herein, we present DBP derivatives **2a–d** with thioether substituents in the 5,10-positions with low LUMO energies and their properties in n-channel OFETs. The LUMO energies of **2a–d** lay between −3.16 and −3.47 eV. Through oxidation to sulfone **3**, the LUMO could be further lowered to −3.94 eV. FET measurements on well-aligned crystals, obtained using the droplet-pinned crystallization method, gave n-channel (electron) mobilities of up to 0.18 $cm^2 V^{-1} s^{-1}$.[26–28] Up to date, these are the highest reported values for n-channel conduction in DBP derivatives.[21,22]

The advantages of incorporating sulphur atoms into organic semiconductors have long been recognized in that thienoacenes are excellent p-type, hole-conducting molecules.[29] Compared to acenes, the incorporation of sulphur atoms typically leads to a lowering of the HOMO energy and thus a higher stability towards oxidation. Strong van-der-Waals interactions between sulphur atoms favour close molecular

[a] Institute for Organic Chemistry, University of Freiburg, Albertstraße 21, 79104 Freiburg, Germany. *E-mail: besser@oc.uni-freiburg.de.
[b] MOE Key Laboratory of Macromolecule Synthesis and Functionalization, State Key Laboratory of Silicon Materials, Department of Polymer Science and Engineering, Zhejiang University, Hangzhou, 310027, P. R. China. *E-mail: hanying_li@zju.edu.cn.
[c] Institute for Inorganic Chemistry, University of Freiburg, Albertstraße 21, 79104 Freiburg

Electronic Supplementary Information (ESI) available: Additional synthetic procedures, CVs, NMR spectra, TGA und DSC measurements, X-ray crystallographic data for **2b** and **2c**, Cartesian coordinates of calculated structures and images of crystals grown by the DPC method of **2c**, **2d** and **3**. See DOI: 10.1039/x0xx00000x

View Article Online
DOI: 10.1039/C8TC00970H

packing in the solid state,[30] advantageous for charge transport in OFETs.

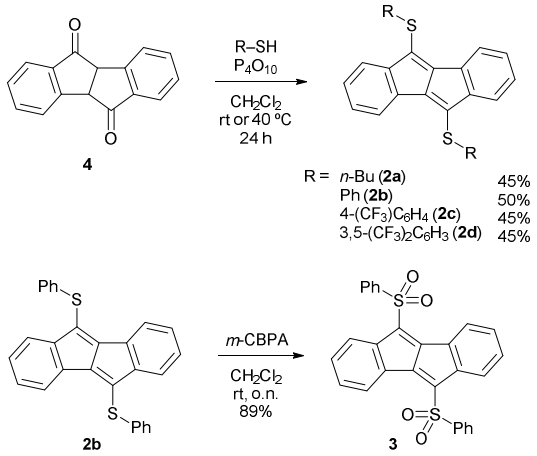

Scheme 1 Synthesis of thio-DBPs **2a–d** and sulfone **3**.

A thio-substituted DBP has been reported only once before,[31] however, no optoelectronic data was acquired, and the synthesis was rather lengthy. The synthesis of thio-DBPs **2a–d**, on the other hand, is facile and can be achieved in one step from diphenyl succindandione (**4**, Scheme 1) or in three steps from commercially available phenylacetic acid.

Results and discussion

Synthesis

Reacting diphenyl succindandione (**4**, for synthesis see ESI) with the corresponding thiol in the presence of phosphorus pentoxide afforded thio-DBPs **2a–d** in yields of 45–50% as red-coloured solids (Scheme 1). Oxidation of phenyl-substituted **2b** with *meta*-chloroperoxybenzoic acid led to sulfone **3** in high yield of 89%. Thio-DBPs **2a–d** showed high thermal stability of up to 312 °C ($T_{d,10\%}$), as measured by thermal gravimetric analysis. In differential scanning calorimetry (DSC) measurements, a melting and recrystallization point was observed for **2b–d**, but not for **2a**, which exhibited no recrystallization. For sulfone **3**, decomposition started at 289 °C ($T_{d,10\%}$) and no phase transition was visible in the DSC curve (see ESI for more information).

Solid-state structures

Layering of a CH_2Cl_2 solution with *n*-pentane or acetonitrile provided single crystals suitable for X-ray diffraction analysis of thio-DBPs **2b** and **2c** (Fig. 2). While the sulfur atoms lie in the plane of the DBP units, the S-aryl groups are rotated by 61.5° for **2b** and 61.9°/63.9° for **2c** relative to the plane of the DBP core. The molecules of **2c** pack in a one-dimensional π-stacked structure with distances between the DBP units of 3.504 Å, which lie in the range of π-π-interactions (Fig. 2b). In the π-stacking directions, the molecules are displaced by 3.16 Å. **2b**, on the other hand, shows a herringbone packing in the solid state (Fig. 2d). In the π-stacking direction, the distance between two DBP units amounts to 3.254 Å (Fig. 2e), and the molecules are displaced from each other by 4.47 Å.

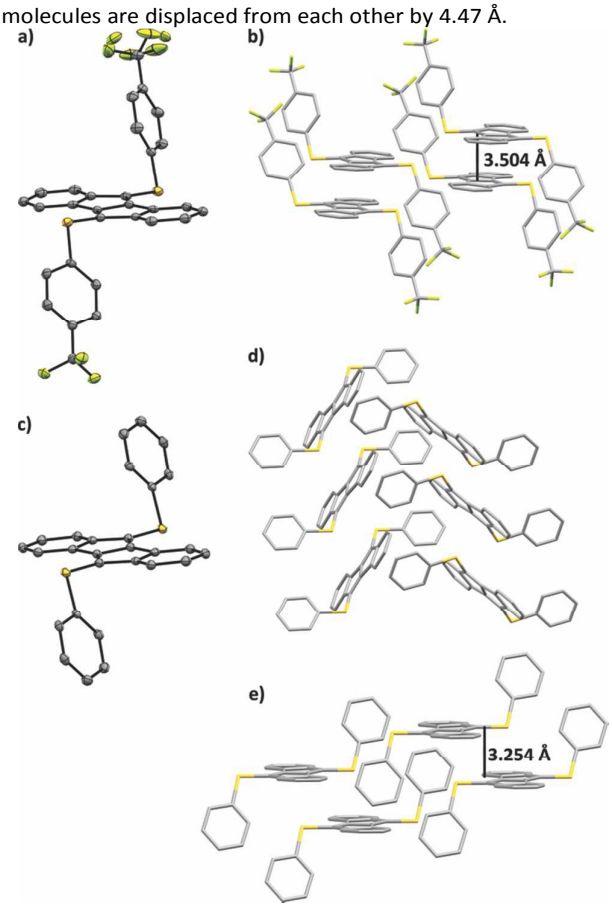

Fig. 2 Molecular structure and packing of **2c** (a, b) and **2b** (c–e) in the solid state (hydrogen atoms are omitted for clarity; in a and c, displacement ellipsoids are shown at 50% probability).

Electrochemical and optical properties

Cyclic voltammetry measurements showed amphoteric redox behaviour for thio-DBPs **2a–c**, where each featured a reversible reduction and oxidation (Fig. 3 and Table 1), only **2d** showed an irreversible oxidation. Sulfone **3** displayed two reversible reduction waves, but no oxidation was visible in the electrochemical window of the solvent (CH_2Cl_2 or THF). HOMO and LUMO energies (Table 1) were obtained from the onsets of the first oxidation/reduction peaks *vs*. Fc/Fc^+, assuming an ionization energy of 4.8 eV for ferrocene.[32] Thio-DBPs **2a–d** showed LUMO energies between −3.16 eV for **2a** and −3.47 eV for **2d**. The presence of the sulfone moieties in **3** significantly lowered its LUMO energy to −3.94 eV. The HOMO energies of thio-DBPs **2a–d** lay between −5.38 and −5.81 eV. DFT calculations provided orbital energies for comparison. The B3LYP[33]-functional was used in combination with D3[34] and the def2-TZVP[35,36] basis set (Fig. 4). The calculated HOMO energies lie reasonably close but below the experimental ones, while the LUMO energies were overestimated in the calculations.

View Article Online
DOI: 10.1039/C8TC00970H
Journal of Materials Chemistry C ARTICLE

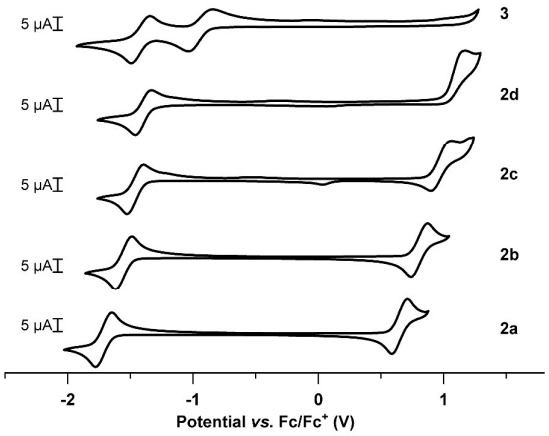

Fig. 3 Cyclic voltammograms of thio-DBPs **2a–d** and sulfone **3** (1 mM in CH_2Cl_2, 0.1 M n-Bu_4NPF_6, scan rate 0.1 V s^{-1}, glassy carbon electrode).

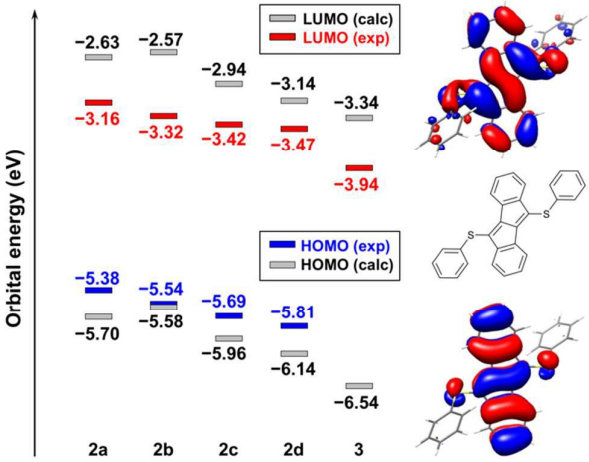

Fig. 4 Energy diagram of experimental (from CV measurements in solution, determined from the onset of the first reduction/oxidation peak *vs.* Fc/Fc^+, assuming an ionization energy of 4.8 eV for ferrocene[32]) and calculated (B3LYP-D3/def2-TZVP) HOMO/LUMO energies of thio-DBPs **2a–d** and sulfone **3**. For calculations the *n*-butyl groups of **2a** were replaced with methyl groups denoted with an asterisk (**2***).

The HOMOs in **2a–d** (exemplarily shown for **2b** in Fig. 4) are localized on the DBP core with some contributions from the sulphur atoms. In comparison, the LUMOs show a much higher contribution of the thioether substituents. This explains the significant influence of the thioether and sulfone groups on the LUMO energies of **2a–d** and **3**.

The absorption spectra of thio-DBPs **2a–d** and sulfone **3** show the transitions expected for DBP derivatives. In centrosymmetric DBP derivatives of C_{2h} symmetry, the HOMO-LUMO transition is forbidden, since both transitions are of a_u symmetry (Laporte's rule).[37] Here, in contrast to other DBP derivatives,[23,24] this transition is not even visible at the onset of the longest wavelength absorption band. The lowest visible absorption bands range from 454 nm (**2a**) to 477 nm (**3**) with extinction coefficients of log ε = 3.94–4.29.

Table 1 Electrochemical and optical data for thio-DBPs **2a–d** and sulfone **3**.

	$E_{red\ 1/2}$ (V)	$E_{ox\ 1/2}$ (V)	E_{HOMO} (eV)[a]	E_{LUMO} (eV)[a]	E_g (eV)	E_g (opt) (eV)[b]
2a	−1.71	0.65	−5.38	−3.16	2.22	1.92
2b	−1.55	0.81	−5.54	−3.32	2.22	1.90
2c	−1.46	0.98	−5.69	−3.42	2.27	1.85
2d	−1.40	1.17[c]	−5.81	−3.47	2.34	1.85
3	−1.42 −0.94	-	-	−3.94	-	1.86

[a]From the onset of the reduction/oxidation peak *vs.* Fc/Fc^+, assuming an ionization energy of 4.8 eV for ferrocene;[32] [b]from the onset of the longest wavelength absorption band, [c]anodic peak potential.

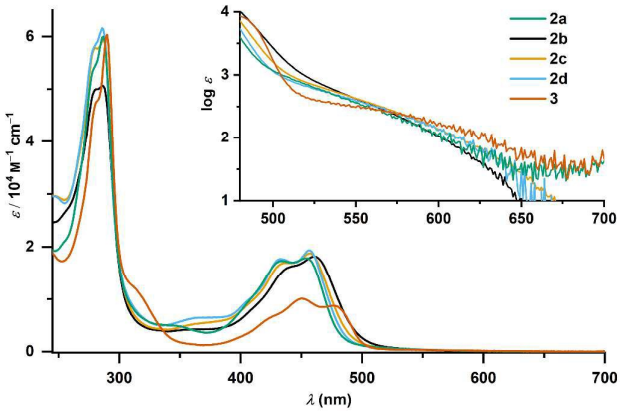

Fig. 5 Absorption spectra of thio-DBPs **2a–d** and sulfone **3** in CH_2Cl_2 solution (Inset: longest wavelength absorption plotted on a logarithmic scale).

The second lowest energy transitions appear with maxima between 433 and 450 nm, while the global absorption maxima are found between 286 and 290 nm with extinction coefficients of log ε = 4.70–4.79.

OFET measurements

The relatively low LUMO levels of the thio-DBPs are a good requisite for n-channel conduction, especially in the cases of **2c** (−3.42 eV), **2d** (−3.47 eV) and sulfone **3** (−3.94 eV). Next, we proceeded to examine the electron transport properties of these DBP derivatives. For **2c**, **2d** and **3**, we obtained well-aligned crystals that were suitable for OFET fabrication using the droplet-pinned crystallization (DPC) method (see ESI for details, Fig. S31).[26–28] OFETs were fabricated with Ag as the source and drain electrodes (Fig. 6c, inset) and tested in the saturation regime under N_2 atmosphere. Compared to commonly employed Au electrodes, Ag has a lower work function that better matches the LUMO energies of **2c**, **d** and **3**. OFETs based on the three compounds all exhibited n-channel behaviour. The corresponding gate modulation is clearly shown by the transfer (Fig. 6a–c) and output characteristics (Fig. 6d–f). The electron mobility, on-to-off current ratios (I_{on}/I_{off}) and threshold voltages (V_T) were

View Article Online
DOI: 10.1039/C8TC00970H

extracted (Table 2), and histograms of electron mobilities are plotted in Fig. 6g–i.

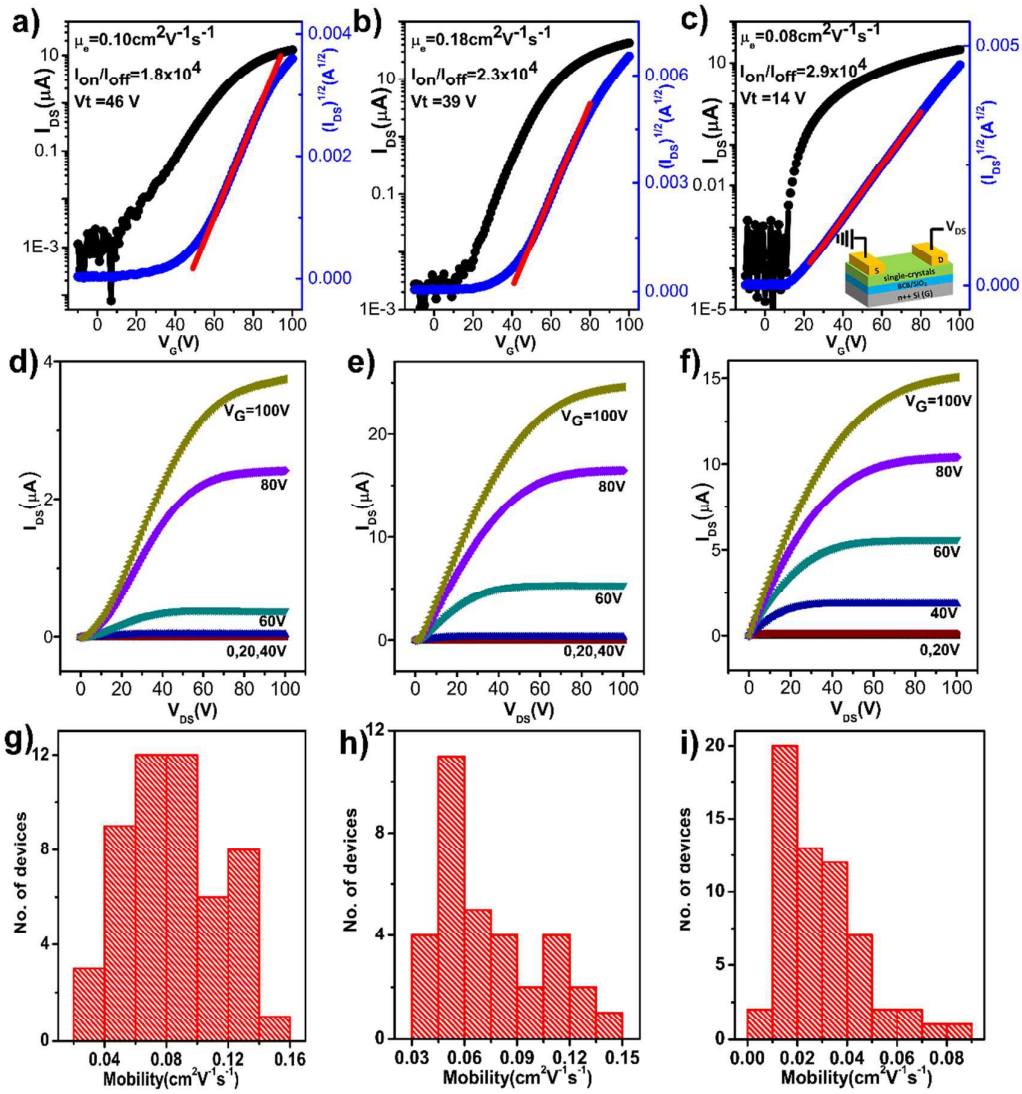

Fig. 6 FET characteristics of the **2c** (a, d and g), **2d** (b, e and h) and **3** crystals (c, f and i). (a–c) Typical transfer characteristics (V_{DS} = 100 V). Inset in c): schematic representation of the FET configuration, where S is the source, D the drain and G the gate. (d–f) Typical output characteristics. (g–i) Histograms of the electron mobility from 51, 35 and 60 devices, respectively.

Table 2 FET characteristics of **2c**, **d** and **3** crystals.

Compound	Mobility (cm^{2}V^{-1}s^{-1})	V_t (V)	I_{on}/I_{off}
2c	$\mu_{average}$ = 8.4×10^{-2} ± 3.1×10^{-2} (range: 3.2×10^{-2} to 1.4×10^{-1})	27–73	>10^3
2d	$\mu_{average}$ = 8.2×10^{-2} ± 3.6×10^{-2} (range: 3.8×10^{-2} to 1.8×10^{-1})	16–41	>10^3
3	$\mu_{average}$ = 2.9×10^{-2} ± 1.7×10^{-2} (range: 4.5×10^{-3} to 8.7×10^{-2})	12–72	>10^2

The electron mobilities for the three crystals are similar, with the highest value of 0.18 cm^2 V^{-1} s^{-1} measured for **2d** (0.10 cm^2 V^{-1} s^{-1} for **2c** and 0.08 cm^2 V^{-1} s^{-1} for **3**). In comparison, the output characteristics (Fig. 6f) for **3** exhibited a better linearity at low V_{DS} region, indicating of better electron injection that is associated with its lower LUMO energy level.[38] Although the mobility achieved is relatively low as compared to that of state-of-the-art n-channel materials,[39–41] higher performance is expected for the new n-channel skeleton of the DBP unit through expanding the side chain structures as well as by crystal engineering. For example, AFM images show that the obtained crystals are not expressed by smooth and flat terraces (Fig. S31c, f, i), indicative of the non-intimate contact between the crystals and the device substrates that is detrimental to the electron-conductive channel. Further work is needed towards achieving smooth crystalline surfaces by chemically modifying the DBP cores to promote dense molecular packing.

View Article Online
DOI: 10.1039/C8TC00970H
Journal of Materials Chemistry C ARTICLE

Conclusions

In conclusion, we have demonstrated thioether- and sulfone-substituted DBPs **2a–d** and **3** with low-lying LUMO energy levels for n-channel conduction in field-effect transistors (FETs). The molecular structures in the solid state showed a one-dimensional π-stacking or herringbone packing mode with close intermolecular distances between the DBP cores. The three derivatives with the lowest LUMO energies, **2c**, **d** and **3**, were used in FETs as well-aligned crystals and displayed n-channel (electron) mobilities of up to 0.18 $cm^2 V^{-1} s^{-1}$. Our synthetic strategy provides facile access to a variety of thioether- and sulfone-functionalized DBPs.

Experimental

Materials and methods

Details on materials and methods can be found in the ESI.

Synthetic procedures

Synthesis of ketone 4. Diphenylsuccinic acid (**6**, 5.00 g, 18.5 mmol) was placed in a dried Schlenk tube. CF_3SO_3H (30 mL, 50 g, 340 mol, 18 eq.) was transferred into the tube using a PTFE cannula. The tube was sealed, and the mixture was heated to 75 °C and stirred at that temperature for 18 h. The reaction mixture was cooled to rt, poured onto ice (150 mL) and extracted with CH_2Cl_2 (3 × 100 mL). The organic layer was washed with sat. aq. Na_2CO_3 solution (100 mL) and brine (100 mL) and dried over Na_2SO_4. The crude mixture was recrystallized from 2-propanol (400 mL) to yield diketone **4** as a light-yellow solid (2.83 g, 12.1 mmol, 65%). R_f 0.27 (cyclohexane/EtOAc: 6/1); **^{1}H NMR** (400 MHz, $CDCl_3$): δ 7.92 (ddd, *J* = 7.8, 1.0, 0.8 Hz, 1H), 7.71 (ddd, *J* = 7.7, 1.3, 0.8 Hz, 1H), 7.67 (ddd, *J* = 7.8, 7.3, 1.3 Hz, 1H), 7.44 (ddd, *J* = 7.7, 7.3, 1.0 Hz, 1H); **^{13}C NMR** (101 MHz, $CDCl_3$): δ 201.6, 149.9, 135.9, 135.1, 129.2, 126.7, 124.9, 52.7; **HRMS** (pos. APCI): *m/z* calcd for $C_{16}H_{11}O_2$ 235.07536 $[M+H]^+$, found 235.07533.

General procedure for the synthesis of thio-DBPs 2. P_4O_{10} (10 eq.) and diketone **4** were placed in a dried Schlenk tube. The tube was evacuated and backfilled with argon. Anh. CH_2Cl_2 was added, and next the respective thiol (4 eq.) was added to the stirred green suspension. The mixture was stirred at the indicated temperature for 24 h. The mixture was quenched with H_2O, diluted with CH_2Cl_2, and the aq. layer was extracted with CH_2Cl_2 (3 ×). The combined organic layers were washed with 20% aq. NaOH solution (2 ×), dried over Na_2SO_4, and the volatiles were removed under reduced pressure. The crude product was purified by column chromatography on silica gel to yield thio-DBPs **2**.

5,10-bis(butylthio)indeno[2,1-*a*]indene (2a). Following the general procedure, ketone **4** (100 mg, 427 µmol), 1-butanethiol (0.18 mL, 1.7 mmol, 4 eq.), P_4O_{10} (1.2 g, 4.2 mmol, 10 eq.) and CH_2Cl_2 (11 mL) were stirred at 40 °C for 24 h. Thio-DBP **2a** was obtained after flash chromatography (cyclohexane/CH_2Cl_2: 1/0 to 20/1) as a red solid (73.1 mg, 193 µmol, 45%). R_f 0.22 (cyclohexane); **^{1}H NMR** (400 MHz, $CDCl_3$): δ 7.40–7.35 (m, 2H), 7.13–7.08 (m, 2H), 7.00–6.94 (m, 4H), 3.06–3.01 (m, 4H), 1.73–1.61 (m, 4H), 1.50–1.40 (m, 4H), 0.90 (t, *J* = 7.4 Hz, 6H); **^{13}C NMR** (101 MHz, $CDCl_3$): δ 149.4, 146.6, 135.1, 134.2, 127.9, 127.7, 122.9, 121.9, 34.0, 32.7, 21.9, 13.8; **HRMS** (pos. APCI): *m/z* calcd for $C_{24}H_{27}S_2$ 379.1549 $[M+H]^+$, found 379.1548.

5,10-bis(phenylthio)indeno[2,1-*a*]indene (2b). Following general procedure, ketone **4** (35.1 mg, 150 µmol), thiophenol (60 µL, 0.58 mmol, 4 eq.), P_4O_{10} (0.56 g, 2.0 mmol, 13 eq.) and CH_2Cl_2 (7.5 mL) were stirred at rt for 24 h. Thio-DBP **2b** was obtained after flash chromatography (hot cyclohexane) as a red crystalline solid (31.3 mg, 74.8 µmol, 50%). R_f 0.20 (cyclohexane); **^{1}H NMR** (400 MHz, $CDCl_3$): δ 7.52–7.47 (m, 4H), 7.33–7.23 (m, 6H), 6.83–6.75 (m, 6H), 6.68–6.64 (m, 2H); **^{13}C NMR** (101 MHz, $CDCl_3$): δ 148.2, 146.3, 133.8, 133.2, 132.5, 130.5, 129.3, 127.8, 127.6, 127.2, 123.2, 122.2; **HRMS** (neg. APCI): *m/z* calcd for $C_{28}H_{18}S_2$ 418.0855 $[M]^{\bullet-}$, found 418.0854.

5,10-bis((4-(trifluoromethyl)phenyl)thio)indeno[2,1-*a*]indene (2c). Following the general procedure, ketone **4** (48.5 mg, 207 µmol), 4-(trifluoromethyl)thiophenol (115 µL, 0.839 mmol, 4 eq.), P_4O_{10} (0.50 g, 1.8 mmol, 8 eq.) and CH_2Cl_2 (5 mL) were stirred at rt for 24 h and at 40 °C for 2 h. Thio-DBP **2c** was obtained after flash chromatography (cyclohexane) as a red crystalline solid (52 mg, 94 µmol, 45%). R_f 0.29 (cyclohexane); **^{1}H NMR** (500 MHz, $CDCl_3$): δ 7.55 (s, 8H), 6.96–6.92 (m, 2H), 6.87–6.82 (m, 4H), 6.69–6.65 (m, 2H); **^{13}C NMR** (126 MHz, $CDCl_3$): δ 148.4, 148.0, 138.7, 133.5, 131.2, 129.5, 129.0 (q, $^2J_{CF}$ = 32.9 Hz), 128.8, 128.2, 126.2 (q, $^3J_{CF}$ = 3.5 Hz), 124.0 (q, $^1J_{CF}$ = 271.6 Hz), 123.6, 122.5; **^{19}F NMR** (471 MHz, $CDCl_3$): δ −62.59; **HRMS** (pos. APCI): *m/z* calcd for $C_{30}H_{17}F_6S_2$ 555.0670 $[M+H]^+$, found 555.0673.

5,10-bis((3,5-bis(trifluoromethyl)phenyl)thio)indeno[2,1-*a*]indene (2d). Following the general procedure, ketone **4** (50.9 mg, 217 µmol), 3,5-bis(trifluoromethyl)thiophenol (0.15 mL, 0.89 mmol, 4 eq.), P_4O_{10} (0.60 g, 2.1 mmol, 10 eq.) and CH_2Cl_2 (6 mL) were stirred at 40 °C for 24 h. Thio-DBP **2d** was obtained after flash chromatography (cyclohexane/CH_2Cl_2: 1/0 to 20/1) as a red solid (66.8 mg, 96.7 µmol, 45%). R_f 0.33 (cyclohexane); **^{1}H NMR** (500 MHz, $CDCl_3$): δ 7.84 (s, 4H), 7.73 (s, 2H), 7.01–6.98 (m, 2H), 6.91–6.84 (m, 4H), 6.62–6.59 (m, 2H); **^{13}C NMR** (126 MHz, $CDCl_3$): δ 149.0, 147.4, 137.2, 133.1, 132.8 (q, $^2J_{CF}$ = 33.5 Hz), 130.0, 129.2, 128.9 (q, $^3J_{CF}$ = 3.3 Hz), 128.6, 123.9, 122.9 (q, $^1J_{CF}$ = 273.2 Hz), 122.5, 120.7 (sept, $^3J_{CF}$ = 3.8 Hz); **^{19}F NMR** (471 MHz, $CDCl_3$): δ −63.14; **HRMS** (pos. APCI): *m/z* calcd for $C_{32}H_{15}F_{12}S_2$ 691.0418 $[M+H]^+$, found 691.0420.

Synthesis of 5,10-bis(phenylsulfonyl)indeno[2,1-*a*]indene (3). Thio-DBP **2b** (46.6 mg, 111 µmol) was dissolved in CH_2Cl_2

View Article Online
DOI: 10.1039/C8TC00970H

(11 mL). *m*-CPBA (70 wt% in H_2O, 220 mg, 0.892 mmol, 8 eq.) was added, and the mixture was stirred at rt for 19 h. The mixture was quenched with sat. aq. $NaHCO_3$ solution (4 mL), and 10% aq. NaOH solution (10 mL) was added. The aq. layer was extracted with CH_2Cl_2 (2 × 15 mL), dried over Na_2SO_4, and the volatiles were removed under reduced pressure. Sulfone **3** was obtained after flash chromatography (siliga gel, CH_2Cl_2/cyclohexane: 3/1) as a red solid (48.2 mg, 98.9 µmol, 89%). R_f 0.28 (CH_2Cl_2/cyclohexane 2/1); **^{1}H NMR** (400 MHz, CD_2Cl_2): δ 8.09–8.00 (m, 2H), 8.04–7.95 (m, 4H), 7.70–7.65 (m, 2H), 7.61–7.51 (m, 4H), 7.39–7.33 (m, 2H), 7.09–6.97 (m, 4H); **^{13}C NMR** (101 MHz, CD_2Cl_2): δ 151.1, 145.6, 140.6, 140.5, 134.9, 132.0, 131.1, 130.2, 130.1, 129.2, 127.7, 124.7; **HRMS** (pos. ESI): *m/z* calcd for $C_{28}H_{18}O_4S_2Na$ 505.0539 $[M+Na]^+$, found 505.0542.

FET device fabrication

Crystals for FETs were grown on a divinyltetramethyldisiloxane-bis(benzocyclobutene) (BCB)[42]-coated highly doped silicon wafer (1 cm^2) with 300 nm thermally oxidized SiO_2, using the DPC method.[26–28] BCB (Dow Chemicals) thin layers were spin-coated from a mesitylene (Fluka) solution ($V_{BCB}/V_{mesitylene}$ = 1:30) and then thermally annealed in a N_2 glovebox.

Crystals were grown *in situ* on substrates for FETs. A solution (20 mL) was dropped onto the substrate and a piece of silicon wafer (0.4 × 0.4 cm^2, pinner) on the substrate was used to pin the solution droplet. The substrate was placed on a Teflon slide inside a Petri dish (35 × 10 mm) sealed with parafilm. The crystals were allowed to grow over 40 min on a hotplate (40±1 °C for **2c**, 35±1 °C for **2d**, 25±1 °C for **3**). **2c** crystals were grown from *m*-xylene (Sigma-Aldrich) at 0.4 mg mL^{-1}, **2d** crystals were grown from heptane (TCI) at 0.2 mg mL^{-1}, and **3** crystals were grown from mixed solvents of *m*-xylene and chloroform (Ourchem) ($V_{m\text{-xylene}}/V_{chloroform}$ = 1:2) at 0.2 mg mL^{-1}.The crystal morphologies were characterized by optical microscopy (OM, Nikon LV100 POL, Nikon) and atomic force microscopy (AFM, Veeco 3D, Veeco). FETs were constructed by depositing top-contact source and drain electrodes (120 nm Ag for **2c** and 100 nm Ag for **2d** and **3**, according to the different thicknesses of each type of crystals) in a bottom-gated configuration through a shadow mask with the channel length (*L*) and width (*W*) of 50 mm and 1 mm. The real *W*/*L* values were measured to calculate the mobility values. Especially for **2c** and **3**, the crystals did not cover the whole channel, and *W* was measured from the contacting area of the crystals that cross the source and drain electrodes. Current-voltage characteristics of the devices were measured using a Keithley 4200-SCS semiconductor parameter analyzer (Keithley) in a N_2 glovebox. The measured capacitance of the BCB-covered SiO_2/Si substrates was 11 nF cm^{-2}, and this value was used for mobility calculations.

DFT calculations

To increase computational speed, the butyl groups in **2a** were replaced with methyl groups. This is indicated by an asterisk (**2a***). TDDFT calculations were performed with the TURBOMOLE v7.2.1 program package.[43] The resolution-of-identity (RI, RIJDX for SP)[44,45] approximation for the Coulomb integrals was used in all DFT calculations employing matching auxiliary basis sets def2-XVP/J.[46] Further, the D3 dispersion correction scheme[34,47] with the Becke-Johnson damping function was applied.[48–50] The geometries of **2a***, **2b–d** and **3** were optimized without symmetry restrictions at the PBEh-3c[51]-D3/def2-mSVP level followed by harmonic vibrational frequency analyses to confirm minima as stationary points. Vertical excitation energies were calculated with TDDFT using the B3LYP[33,52] functionals with the def2-TZVP basis set.[36]

Conflicts of interest

There are no conflicts to declare.

Acknowledgements

Generous support by the German Research Foundation (Emmy Noether grant ES 361/2-1 and grant No. INST 40/467-1 FUGG), the state of Baden-Württemberg through bwHPC and the National Natural Science Foundation of China (51625304, 51461165301) is gratefully acknowledged.

Notes and references

1 R. Gleiter and G. Haberhauer, *Aromaticity and Other Conjugation Effects*, Wiley-VCH, Weinheim, Germany, 2012.
2 Q. Xie, E. Perez-Cordero and L. Echegoyen, *J. Am. Chem. Soc.*, 1992, **114**, 3978–3980.
3 B. Yuan, J. Zhuang, K. M. Kirmess, C. N. Bridgmohan, A. C. Whalley, L. Wang and K. N. Plunkett, *J. Org. Chem.*, 2016, **81**, 8312–8318.
4 G. Dai, J. Chang, J. Luo, S. Dong, N. Aratani, B. Zheng, K. W. Huang, H. Yamada and C. Chi, *Angew. Chem. Int. Ed.*, 2016, **55**, 2693–2696.
5 S. Kato, S. Kuwako, N. Takahashi, T. Kijima and Y. Nakamura, *J. Org. Chem.*, 2016, **81**, 7700–7710.
6 H. Oshima, A. Fukazawa and S. Yamaguchi, *Angew. Chem. Int. Ed.*, 2017, **56**, 3270–3274.
7 D. T. Chase, A. G. Fix, B. D. Rose, C. D. Weber, S. Nobusue, C. E. Stockwell, L. N. Zakharov, M. C. Lonergan and M. M. Haley, *Angew. Chem. Int. Ed.*, 2011, **50**, 11103–11106.
8 D. T. Chase, A. G. Fix, S. J. Kang, B. D. Rose, C. D. Weber, Y. Zhong, L. N. Zakharov, M. C. Lonergan, C. Nuckolls and M. M. Haley, *J. Am. Chem. Soc.*, 2012, **134**, 10349–10352.
9 H. Xin, C. Ge, X. Jiao, X. Yang, K. Rundel, C. R. McNeill and X. Gao, *Angew. Chem. Int. Ed.*, 2018, **57**, 1322–1326.
10 H. Xin and X. Gao, *ChemPlusChem*, 2017, **82**, 945–956.
11 J. D. Wood, J. L. Jellison, A. D. Finke, L. Wang and K. N. Plunkett, *J. Am. Chem. Soc.*, 2012, **134**, 15783–15789.
12 X. Gao and Y. Hu, *J. Mater. Chem. C*, 2014, **2**, 3099–3117.
13 Y. Zhao, Y. Guo and Y. Liu, *Adv. Mater.*, 2013, **25**, 5372–5391.

View Article Online
DOI: 10.1039/C8TC00970H
Journal of Materials Chemistry C ARTICLE

14 Q. Meng and W. Hu, *Phys. Chem. Chem. Phys.*, 2012, **14**, 14152.
15 C. R. Newman, C. D. Frisbie, A. da S. F. Demetrio, J.-L. Brédas, P. C. Ewbank, K. R. Mann, S. Filho and J. Bre, *Chem. Mater.*, 2004, **16**, 4436–4451.
16 J. Zaumseil and H. Sirringhaus, *Chem. Rev.*, 2007, **107**, 1296–1323.
17 G. Dai, J. Chang, W. Zhang, S. Bai, K.-W. Huang, J. Xu and C. Chi, *Chem. Commun.*, 2015, **51**, 503–506.
18 C. Liu, S. Xu, W. Zhu, X. Zhu, W. Hu, Z. Li and Z. Wang, *Chem. Eur. J.*, 2015, **21**, 17016–17022.
19 C. Li, C. Liu, Y. Li, X. Zhu and Z. Wang, *Chem. Commun.*, 2015, **51**, 693–696.
20 T. Kawase, T. Fujiwara, C. Kitamura, A. Konishi, Y. Hirao, K. Matsumoto, H. Kurata, T. Kubo, S. Shinamura, H. Mori, E. Miyazaki and K. Takimiya, *Angew. Chem. Int. Ed.*, 2010, **49**, 7728–7732.
21 G. Dai, J. Chang, L. Jing and C. Chi, *J. Mater. Chem. C*, 2016, **4**, 8758–8764.
22 M. Nakano, I. Osaka and K. Takimiya, *J. Mater. Chem. C*, 2015, **3**, 283–290.
23 D. C. Grenz, M. Schmidt, D. Kratzert and B. Esser, *J. Org. Chem.*, 2018, **83**, 656–663.
24 J. Wilbuer, D. C. Grenz, G. Schnakenburg and B. Esser, *Org. Chem. Front.*, 2017, **4**, 658–663.
25 M. Hermann, D. Wassy, D. Kratzert and B. Esser, 2018, *submitted*.
26 H. Li, B. C. K. Tee, J. J. Cha, Y. Cui, J. W. Chung, S. Y. Lee and Z. Bao, *J. Am. Chem. Soc.*, 2012, **134**, 2760–2765.
27 H. Li, C. Fan, M. Vosgueritchian, B. C.-K. Tee and H. Chen, *J. Mater. Chem. C*, 2014, **2**, 3617.
28 Q.-F. Li, S. Liu, H.-Z. Chen and H.-Y. Li, *Chinese Chem. Lett.*, 2016, **27**, 1421–1428.
29 K. Takimiya, S. Shinamura, I. Osaka and E. Miyazaki, *Adv. Mater.*, 2011, **23**, 4347–4370.
30 R. Gleiter, G. Haberhauer, D. B. Werz, F. Rominger and C. Bleiholder, *Chem. Rev.*, 2018, acs.chemrev.7b00449.
31 F. Xu, L. Peng, K. Wakamatsu, A. Orita and J. Otera, *Chem. Lett.*, 2014, **43**, 1548–1550.
32 B. W. D'Andrade, S. Datta, S. R. Forrest, P. Djurovich, E. Polikarpov and M. E. Thompson, *Org. Electron.*, 2005, **6**, 11–20.
33 A. D. Becke, *J. Chem. Phys.*, 1993, **98**, 5648–5652.
34 S. Grimme, J. Antony, S. Ehrlich and H. Krieg, *J. Chem. Phys.*, 2010, **132**, 154104.
35 F. Weigend and R. Ahlrichs, *Phys. Chem. Chem. Phys.*, 2005, **7**, 3297–305.
36 A. Schäfer, C. Huber and R. Ahlrichs, *J. Chem. Phys.*, 1994, **100**, 5829–5835.
37 C. G. Wermuth, C. R. Ganellin, P. Lindberg and L. A. Mitscher, *Pure Appl. Chem.*, 1979, **51**, 1129–1143.
38 D. Natali and M. Caironi, *Adv. Mater.*, 2012, **24**, 1357–1387.
39 Y.-Q. Zheng, T. Lei, J.-H. Dou, X. Xia, J.-Y. Wang, C.-J. Liu and J. Pei, *Adv. Mater.*, 2016, **28**, 7213–7219.
40 X. Xu, Y. Yao, B. Shan, X. Gu, D. Liu, J. Liu, J. Xu, N. Zhao, W. Hu and Q. Miao, *Adv. Mater.*, 2016, **28**, 5276–5283.
41 G. Xue, J. Wu, C. Fan, S. Liu, Z. Huang, Y. Liu, B. Shan, H. L. Xin, Q. Miao, H. Chen and H. Li, *Mater. Horizons*, 2016, **3**, 119–123.
42 L.-L. Chua, J. Zaumseil, J.-F. Chang, E. C.-W. Ou, P. K.-H. Ho, H. Sirringhaus and R. H. Friend, *Nature*, 2005, **434**, 194–199.
43 TURBOMOLE V7.0 2015, a development of the University of Karlsruhe and Forschungszentrum Karlsruhe GmbH, 1989-2007, TURBOMOLE GmbH, since 2007; available from http://www.turbomole.com.
44 K. Eichkorn, O. Treutler, H. Öhm, M. Häser and R. Ahlrichs, *Chem. Phys. Lett.*, 1995, **240**, 283–290.
45 K. Eichkorn, O. Treutler, H. Öhm, H. Marco and R. Ahlrichs, *Chem. Phys. Lett.*, 1995, **242**, 652–660.
46 F. Weigend, *Phys. Chem. Chem. Phys.*, 2006, **8**, 1057–1065.
47 S. Grimme, S. Ehrlich and L. Goerigk, *J. Comput. Chem.*, 2011, **32**, 1456–1465.
48 E. R. Johnson and A. D. Becke, *J. Chem. Phys.*, 2005, **123**, 24101.
49 E. R. Johnson and A. D. Becke, *J. Chem. Phys.*, 2006, **124**, 174104.
50 A. D. Becke and E. R. Johnson, *J. Chem. Phys.*, 2005, **123**, 154101.
51 S. Grimme, J. G. Brandenburg, C. Bannwarth and A. Hansen, *J. Chem. Phys.*, 2015, **143**, 54107.
52 P. J. Stephens, F. J. Devlin, C. F. Chabalowski and M. J. Frisch, *J. Phys. Chem.*, 1994, **98**, 11623–11627.

View Article Online
DOI: 10.1039/C8TC00970H

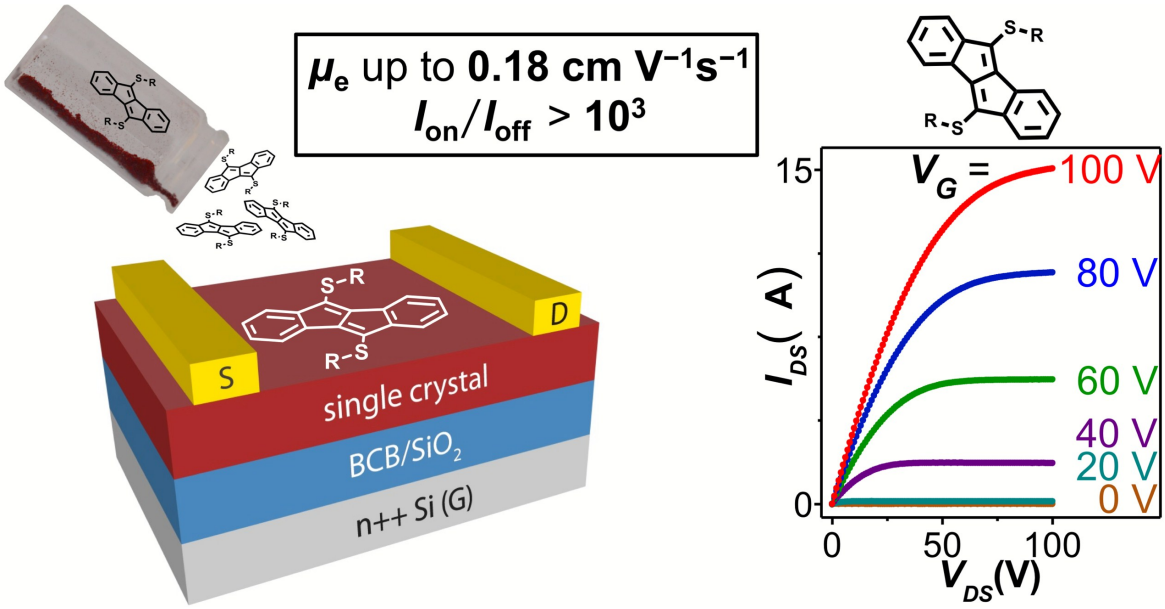

Dibenzo[*a*,*e*]pentalenes, functionalized with thioether or sulfone groups, show high electron mobilities in n-channel OFETs using well-aligned crystals.